

# Photorefraction and complementary grating competition in bipolar transport molecular material

Liming Wang, Man-Kit Ng, and Luping Yu\*

*Department of Chemistry and The James Franck Institute, The University of Chicago, 5735 South Ellis Avenue, Chicago, Illinois 60637*

(Received 28 February 2000)

A comprehensive investigation of the photorefractive properties of an unusual molecular material is reported. This material is a glassy solid that is composed of a multifunctional molecule consisting of a sexithiophene covalently linked with a nonlinear optical chromophore, a methine dye. A net photorefractive gain coefficient of  $70.5 \text{ cm}^{-1}$  and a diffraction efficiency of 18.9% (130  $\mu\text{m}$  thick) were observed. It was found that this material exhibits the competition of complementary holographic gratings that are formed by the space-charge field of two types of photocarriers. Competition of complementary holographic gratings was revealed from the cancellation and revelation of the two types of gratings and is discussed based on a bipolar two-trap photorefractive model. Two transport channels and two trapping centers for photogenerated electrons and holes, respectively, are responsible for the formation of the two complementary gratings. The mobility and the number density of traps for the two types of charged carriers are different; time-of-flight results indicate that the holes have higher mobility than the electrons. A slow, secondary (weak) grating formed by electrons is  $180^\circ$  out of phase with respect to that of the fast, principal one formed by holes. This reduces the net space-charge field, and a cancellation in the index grating was exhibited during the grating formation process. The slow grating could be revealed, and an oscillationlike behavior was shown under the irradiation of a uniform light. The oxidation and reduction potentials of the charge-carrier species explain the microscopic mechanism for the bipolar transport channels. The buildup dynamics of the gratings are discussed in detail.

## I. INTRODUCTION

Both organic and inorganic photorefractive materials have been extensively investigated for applications in data storage and real time information processing.<sup>1-21</sup> Organic photorefractive materials are molecular materials that exhibit weak intermolecular interactions and are typically soft amorphous solids. These characteristics distinguish organic material from inorganic materials in all of the four processes involved in the photorefractive effect. For example, charge carriers are generated through the dissociation of tightly bonded excitons, not via interband ionization. The photogenerated carriers are transported away under an electric field via intersite hopping, thereby experiencing dispersed potential energy. Because of the amorphous and disorderly nature of the transporting molecular network, the depth of the traps in organic materials has a rather dispersed distribution. Furthermore, the electro-optic response is provided by an individual molecular chromophore with an electronic origin.

With the development of new organic photorefractive materials, it is frequently observed that in organic materials the grating buildup and decay does not follow a single exponential function as predicted by the standard model of photorefraction.<sup>22</sup> However, the grating formation and erasure do consist of multiple components with different time constants.<sup>23-27</sup> One of the reasons for this is the existence of a more dispersed distribution of trap levels. Two- or multi-level trap models have been proposed in which photogenerated charge carriers are redistributed in two or more levels, thereby creating superimposed in-phase gratings. Since the trap density, photoexcitation, and recombination rates are generally different for each level, each grating should have different exponential time constants for buildup and decay. Some phenomena, such as cancellation and revelation of the

gratings,<sup>28</sup> were observed in a photorefractive polymeric composite, which is composed of 40 wt.% diethylaminobenzaldehyde-diphenyl hydrazone (DEH) dissolved in Bisphenol A 4,4'-nitroaminotolane. A two-trap model with charge exchange between traps was proposed, assuming that the first type of trap is highly photosensitive and the second type of trap has low photogeneration efficiencies and collects charges liberated from the first type of trap.<sup>28</sup> The movement of the charge from the first trap to the second one is responsible for the grating revelation and cancellation. The unique quasinondestructive reading has been observed in a photorefractive polymeric composite; poly(methyl methacrylate): 1,3-dimethyl-2,2-tetramethylene-5-nitrobenzimidazole:  $\text{C}_{60}$ . The properties were explained by a two-trap-level model in which the two levels were populated sequentially. The intensity-dependent decay rate and the transition were qualitatively mimicked.<sup>29</sup> In these models, only one type of the photogenerated carrier (hole) was involved. These special phenomena are the results of the traps' intercommunication. In another study on a photorefractive polymeric composite comprised of a methyl methacrylate copolymer with a side-chain nonlinear optical (NLO) chromophore *p*-nitroaniline doped with 30 wt.% DEH,<sup>30</sup> grating competition and revelation was found to be the result of the competition between two gratings with the presence of two types of charges. The primary grating was from the charged carrier hole, while the secondary grating was attributed to residual ionic motion in response to the photorefractive space-charge field.<sup>30</sup>

In this paper, we report a comprehensive investigation of the photorefractive properties of an unusual glassy molecular material that exhibits both sizable photorefractive properties and competition between the complementary holographic gratings. To our knowledge, this material is the first organic

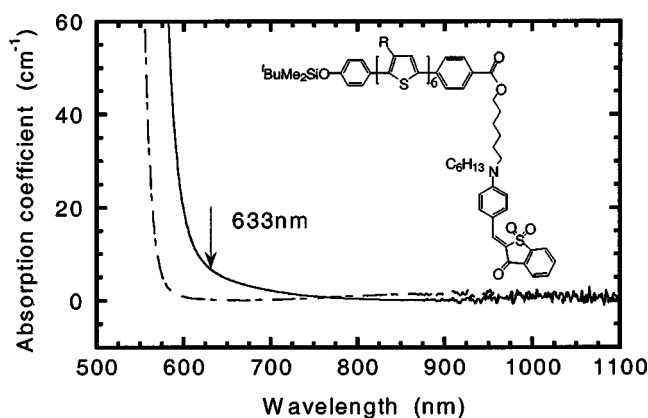


FIG. 1. The structure of the photorefractive molecule containing a sexithiophene derivative and a methine dye (inset), and the absorption spectrum in solid state of the photorefractive molecule (solid line) and that of sexithiophene backbone only (dashed line).

compound to exhibit complementary gratings formed by simultaneous electron-hole transport, although the phenomenon has been extensively studied experimentally<sup>31–36</sup> and theoretically<sup>34,37–40</sup> in inorganic photorefractive crystals.

We will describe the preparation of materials and samples in Sec. II. Section III characterizes the photorefractive properties, the grating cancellation, and revelation behaviors in the recording and erasing processes. Section IV provides evidence for the bipolar transport nature of the material from the mobility measurement in a time-of-flight experiment. In Sec. V, we propose a possible two-channel two-trap molecular model based on the molecular energy levels deduced from electrochemical measurements and known photorefractive theory. We also discuss the dynamics of complementary grating writing and erasing. Section VI summarizes our understanding of the photorefractive properties of the material.

## II. MOLECULAR DESIGN AND SAMPLE PREPARATION

The material studied in this paper contains a sexithiophene derivative covalently linked to an NLO chromophore, a methine dye.<sup>41</sup> The molecular structure of this compound is shown in Fig. 1, and its redox potentials and

band gap are shown in Table I (Compound 1). The sexithiophene derivative was introduced to facilitate hole transport. The free charge carriers are generated by the photoexcitation of the methine dye. This is because the molecule exhibits an absorption coefficient of  $6.42 \text{ cm}^{-1}$  at the wavelength of 633 nm with a dominant contribution from the NLO chromophore, while the absorption coefficient of the sexithiophene segment (Compound 2 in Table I) was estimated to be less than  $0.2 \text{ cm}^{-1}$  as shown in Fig. 1. Therefore, the methine dye plays multiple roles as a photogenerator, NLO chromophore, and an electron transporter. The branched side chains on the thiophene rings were introduced to prevent the materials from crystallizing. The glass transition temperature  $T_g$  of the material is  $-3.2^\circ\text{C}$  as measured by differential scanning calorimetry (TA Instruments, Model DSC-10). It is well known that the refractive index modulation of a low- $T_g$  photorefractive material can be enhanced by the orientation of an NLO chromophore in response to the space-charge field.<sup>42</sup> The refractive index of the material at 632.8 nm is 1.64 measured with a prism coupler (Metricron, Model 2010).

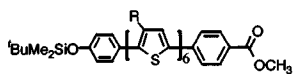
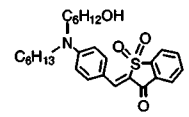
Samples for the volume holographic recording were prepared by applying a concentrated solution of compound 1 in chloroform onto two pieces of indium tin oxide (ITO) glass. After drying at  $80\text{--}90^\circ\text{C}$  on a hot plate for 20 min, the samples were dried thoroughly in a vacuum oven for 16 h at  $60\text{--}70^\circ\text{C}$ . The two pieces were then pressed together with a polyimide spacer ( $125 \mu\text{m}$ ) to maintain a uniform thickness. Samples for photoconductivity and mobility measurements were prepared by the same procedures, except that thinner polyimide spacers ( $25 \mu\text{m}$ ) were used. These films were compressed between either two pieces of ITO glass or one ITO glass and an aluminum plate.

## III. GRATING RECORDING EXPERIMENTS

### A. Experimental techniques

The grating recording experiments (two-beam coupling and four-wave mixing) were conducted by using a radiation of He-Ne laser (Spectra-Physics, Model 127, 632.8 nm). The two grating-writing beams were loosely focused to spots

TABLE I. Structures, redox potentials, with respect to the standard hydrogen electrode (SHE) and band gaps of the three components measured by using electrochemical and photoabsorption methods.

Compound number	Structure	$V_{\text{ox}}$ vs SHE (V)	$V_{\text{red}}$ vs SHE (V)	$V_{\text{red}} - V_{\text{ox}}$ ( $\sim \Delta E_{\text{electrochemical}}$ ) (V)	Photoabsorption edge ( $\sim \Delta E_{\text{optical}}$ ) (eV)
1	Photorefractive Molecule (see Figure 1)	1.02 (1.49 <sup>a</sup> )	0.92	1.94 (2.41 <sup>b</sup> )	2.30
2		1.08	—	—	2.48
3		1.43	0.94	2.37	2.30

<sup>a</sup>assigned as the lowest oxidation potential of methine dye segment.

<sup>b</sup>calculated from difference of redox potentials that are assigned to methine dye ( $a - V_{\text{red}}$ ).

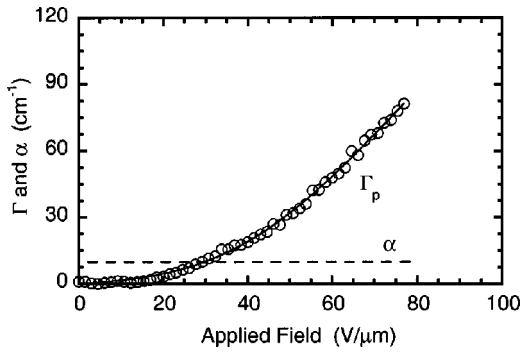


FIG. 2. Photorefractive gain coefficient ( $\Gamma_p$ ) as a function of applied field. The dashed line is the absorption coefficient at the laser wavelength (632.8 nm). The solid line is the theoretical fit using Eq. (3) with  $E_{q \text{ eff}}=94.5 \text{ V}/\mu\text{m}$ .

with a diameter of  $860 \mu\text{m}$  inside of the sample by using a lens of  $500 \text{ mm}$  focus length. In a two-wave-mixing experiment, two  $p$ -polarized laser beams with an equal intensity of  $830 \text{ mW}/\text{cm}^2$  were overlapped in the sample to write the index grating. The incident-crossing angle of the beams is  $7.5^\circ$ , and the film normal was tilted at an angle of  $53^\circ$  with respect to the symmetric axis of the two writing beams to ensure a nonzero projection of the external field in the direction of the grating vector. The transmitted intensities of both beams were detected using two calibrated photodetectors (Newport, Model 1815-C, Photodiode, 818-SL) and were recorded with a personal computer. The photorefractive gains were calculated by using the expression,  $\Gamma = (1/L) \times \ln[\gamma/(2 - \gamma)]$ , where  $L$  is the optical path for the amplified beam, and  $\gamma$  is the beam coupling ratio (the ratio of the signal intensities with and without pump beam). The phase shifts of the index grating with respect to the writing intensity pattern were measured and calculated using the method described by Suter and Günter.<sup>43</sup> In these calculations, the effect of the re-writing during the motion of the grating was taken into consideration. This is because the stage speed was slower ( $7.2 \mu\text{m}/\text{sec}$ ) than the time constant for the index grating buildup time (less than 1 sec). The diffraction efficiency  $\eta$ , which is the ratio of the intensity of diffracted light to that of the incident light, was measured in a degenerate four-wave mixing experiment. Two  $s$ -polarized laser beams with an intensity of  $760 \text{ mW}/\text{cm}^2$  were used as the writing beams, which were overlapped in the tilted sample with an incident-crossing angle of  $8.3^\circ$ . A probe beam is a weak  $p$ -polarized beam with an intensity of  $4.6 \text{ mW}/\text{cm}^2$ , counterpropagating along the direction of one of the writing beams. The spot diameter was reduced to  $620 \mu\text{m}$  with a  $500 \text{ mm}$  focus length lens. To exclude background light, the probe beam was chopped into the frequency of  $317 \text{ Hz}$  and the diffracted signal was amplified with a lockin amplifier (Stanford Research Systems, Model SR510). All of the measurements were controlled by a personal computer (Dell, NetPlex 450/p).

### B. Photorefractive gain coefficient

The photorefractive gain coefficient was measured by a two-beam coupling experiment. A clear asymmetric energy transfer in two-beam coupling experiments was observed. Figure 2 shows the strong dependence of the photorefractive

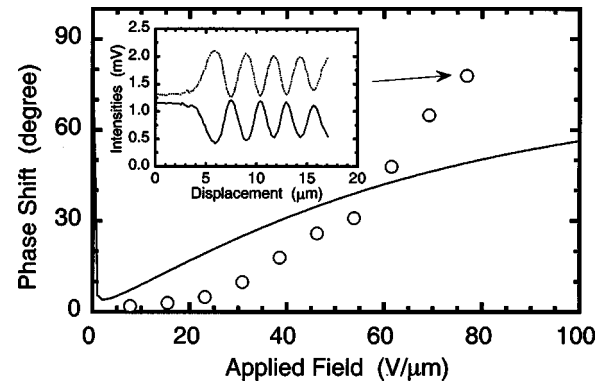


FIG. 3. Phase shift as a function of applied field of steady-state refractive index grating with respect to the writing light intensity grating. The inset is a typical intensity of the two beams when the grating was moved about  $14 \mu\text{m}$  in the direction of the grating vector. The solid line is the theoretical fit using Eq. (3) with  $E_{q \text{ eff}}=99.9 \text{ V}/\mu\text{m}$ .

gain on the applied field. No gain was observed at a zero applied field. The relationship between the photorefractive gain and the applied field is superlinear as a result of the field dependence of photogeneration quantum efficiency and mobility of charge carriers.<sup>44</sup> The largest gain obtained is  $76.9 \text{ cm}^{-1}$  at an applied field of  $77 \text{ V}/\mu\text{m}$ . Since the absorption coefficient of the material was  $6.42 \text{ cm}^{-1}$ , a net optical gain of  $70.4 \text{ cm}^{-1}$  was obtained.

The phase shift of the index grating was found to increase monotonically with the applied field, starting from almost zero at a low field ( $<30 \text{ V}/\mu\text{m}$ ) and increasing to about  $78^\circ$  at  $77 \text{ V}/\mu\text{m}$  (Fig. 3). The typical transmitted intensities of the two coupling beams during the translation of the grating are shown as an inset in Fig. 3. Both the energy transfer and phase shift originated from the nonlocalization of photorefractive grating. The grating could be completely erased and rewritten with good reproducibility.

To measure the dependence of the gain coefficient on the spatial frequency of grating, the tilted angle of the sample normal was kept at  $40^\circ$  with respect to the symmetric axis of the two writing beams, and the inner intersection angle of the two overlapped beams was changed from  $2.6^\circ$  to  $31^\circ$ . This experimental arrangement resulted in the grating spacing varying between  $0.4$  and  $4.4 \mu\text{m}$ , while the field component along the grating vector remained constant under the fixed external field. The gain coefficient increases with the decrease of the spacing, and the maximum is reached at about  $1 \mu\text{m}$ . It then decreases steeply at a small grating space range (Fig. 4).

### C. Diffraction efficiency

The diffraction efficiency was measured with degenerate four-wave-mixing experiments and was also strongly dependent on the applied field (Fig. 5). The index modulation from other mechanisms, including photochemistry, thermorefractive, thermochromism, photochromism, and  $\chi^3$  contribution are negligible because the index modulation from these mechanisms does not depend on the applied field, and some are irreversible without light treatment. A diffraction efficiency of  $19.8\%$  at an applied field of  $77 \text{ V}/\mu\text{m}$  was achieved

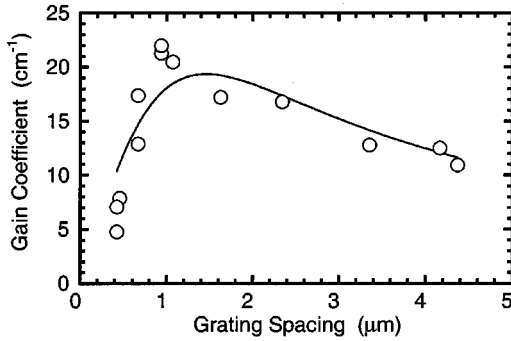


FIG. 4. Gain coefficient as a function of grating spacing measured at an applied field of  $66 \text{ V}/\mu\text{m}$ . The circles are the experimental measurements. The solid line is the theoretical fit using Eq. (3) with  $E_{q \text{ eff}} = 102.6 \text{ V}/\mu\text{m}$ .

in films of  $130 \mu\text{m}$  in thickness. To investigate the influence of grating spacing on grating formation and erasure dynamics, we measured the response times at different beam-incident angles at a constant tilted angle.

#### D. Photorefractive sensitivity and dynamic range

The important advantage of the photorefractive all-optic modulator is its high sensitivity. A large index modulation can be achieved optically by milliwatt total power. Four definitions for the evaluation of photorefractive sensitivity are<sup>1-4</sup>  $S_{n_1} = dn_i/dW_0 \times 1/\alpha$ ,  $S_{n_2} = dn_i/dW_0 = \alpha S_{n_1}$ ,  $S_{\eta_1} = d(\eta^{1/2})/dW_0 \times 1/(\alpha l)$ , and  $S_{\eta_2} = d(\eta^{1/2})/dW_0 \times 1/l = \alpha S_{\eta_1}$ , where  $n_i$  is the refractive index,  $\alpha$  is the absorption coefficient,  $W_0$  is the incident optical energy,  $\eta$  is the diffraction efficiency, and  $l$  is the thickness of the hologram. Since the effective index modulation seen by a  $p$ -polarized probe beam,  $\Delta n$ , is related to the diffraction efficiency  $\eta$  by the expression<sup>17,42</sup>

$$\Delta n = \frac{\lambda (\cos \theta_2 \cos \theta_1)^{1/2} \sin^{-1}(\sqrt{\eta})}{\pi l \cos(\theta_2 - \theta_1)}, \quad (1)$$

where  $\theta_1, \theta_2$  are the internal propagation angles of the reading and diffracted beams in film, respectively. The relation between  $S_{n_1}$  and  $S_{\eta_1}$  is  $S_{\eta_1} = \pi \cos(\theta_2 - \theta_1) / [\lambda (\cos \theta_2 \cos \theta_1)^{1/2}] S_{n_1}$ .

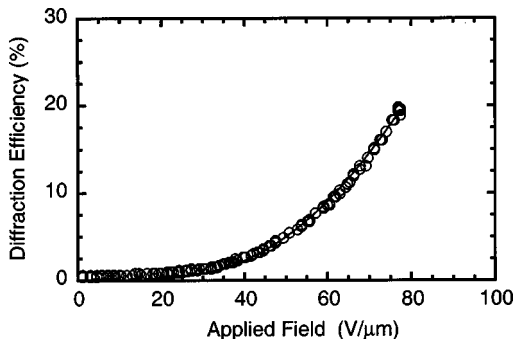


FIG. 5. Dependence of diffraction efficiency on the applied field. The solid line is the theoretical fit using Eq. (3) with  $E_{q \text{ eff}} = 102.6 \text{ V}/\mu\text{m}$ .

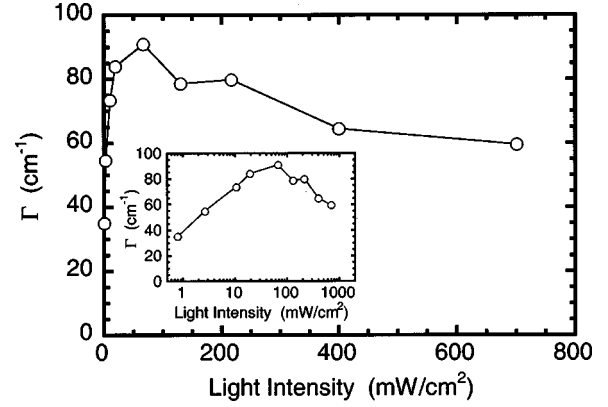


FIG. 6. Photorefractive gain coefficient as a function of the irradiation intensity of each writing beam (the intensity of the two beams remained the same). The inset is the same data, but the horizontal axis is in logarithmic scale.

To study the photorefractive sensitivity, we measured the two-beam coupling gain as a function of the coupling beam intensity (Fig. 6). The intensities of the two beams were changed by rotating the quarter wave plate before the polarizer while equal intensities were maintained during the intensity variation. The optical gain is about  $35 \text{ cm}^{-1}$  when the light intensity is  $1 \text{ mW}/\text{cm}^2$  and increases quickly to its peak of about  $90 \text{ cm}^{-1}$  at the intensity of about  $70 \text{ mW}/\text{cm}^2$ . This is followed by a slight decrease in the high-intensity region. The inset of the same figure depicts the semilogarithmic plot to clarify the low intensity portion. The diffraction efficiency exhibited a similar trend as shown in Fig. 7. The diffraction efficiency climbs fast to about 30% at the light intensity of about  $100 \text{ mW}/\text{cm}^2$ , and then goes down slightly as well. The details at low light intensity can be seen more clearly in the inserted semilogarithmic figure. The diffraction efficiency around  $1 \text{ mW}/\text{cm}^2$  is approximately zero in Fig. 7, while the photorefractive gain of  $36 \text{ cm}^{-1}$  at this intensity is shown in Fig. 6. Since the intensity of the probe beam is comparable to those of the writing beams, the difference is caused by the erasure of the index grating by the homogeneous probe beam. Both intensity dependence behaviors of the gain and diffraction efficiency were reversible during the intensity scan. The photorefractive sensitivities of the sexithiophene derivative at

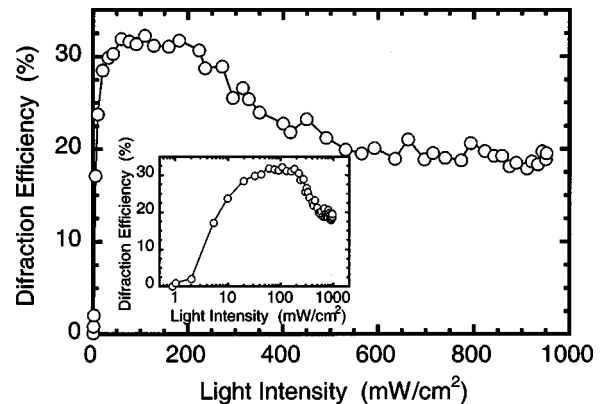


FIG. 7. Diffraction efficiency as a function of the irradiation intensity of each writing beam (the intensity of the two beams remained the same). The inset is the same data, but the horizontal axis is in logarithmic scale.



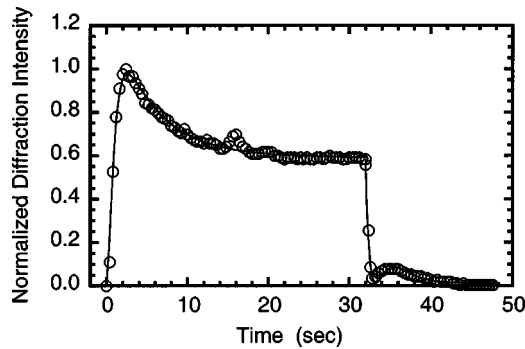


FIG. 8. Diffraction efficiency as a function of time when a grating spacing is  $1.1 \mu\text{m}$  and the applied field is  $77 \text{ V}/\mu\text{m}$ . The writing beams are turned on at  $t=0$ , and one of the writing beams is blocked at  $t=32 \text{ sec}$ . The solid line is a fitting of the data into a biexponential function (Eq. 4).

the intensity of  $80 \text{ mW}/\text{cm}^2$  were determined to be  $S_{n_1} = 18.7 \text{ cm}^3/\text{kJ}$ ,  $S_{n_2} = 120.1 \text{ cm}^2/\text{kJ}$ ,  $S_{\eta_1} = 0.34 \text{ cm}^2/\text{mJ}$ , and  $S_{\eta_2} = 2.2 \text{ cm}/\text{mJ}$ . The maximum refractive index modulation at this intensity was found to be  $0.00075$ .

### E. Relaxation processes

Figure 8 shows the diffraction efficiency variation with time measured at a grating spacing of  $1.1 \mu\text{m}$ . At  $t=0 \text{ sec}$ , two writing beams were overlapped inside the sample. The diffraction signal increased rapidly to a maximum value and then decreased gradually until a steady-state diffraction efficiency was reached. At  $t=32 \text{ sec}$ , the sample was illuminated only by a uniform light by blocking one of the writing beams. The diffraction efficiency decayed exponentially until it was nearly zero, appeared again for a short time, and eventually disappeared completely. In another measurement, one of the writing beams was blocked before the maximum diffraction efficiency was reached. The grating was exponentially erased as predicted by the standard photorefractive theory.

These phenomena are due to the cancellation and revelation of two types of gratings, as has been observed in several inorganic crystals, such as  $\text{Bi}_{12}\text{TiO}_{12}$ ,  $\text{Sn}_2\text{P}_2\text{S}_6$ , and  $\text{Bi}_4\text{Ti}_3\text{O}_{12}$ .<sup>31,33,36,45</sup> We propose that the two sets of photorefractive gratings are formed by two types of photoexcited charge carriers: electrons and holes. This is because of the bipolar transport property of this molecular photorefractive material, and the existence of two types of trap centers for the holes and electrons. The sexithiophene moieties of compound 1 provide a transport channel for the hole migration, while the methine dye acts as another transport channel for the electron migration because of the presence of a strong electron-withdrawing group.

When writing the gratings, a fast grating is initially built up through trapped holes because of their higher mobility (as shown later). This process results in the initial quick rise in the diffraction efficiency. Thus, the erasure of the grating at this stage shows a single exponential decay. If the grating writing continues for a longer time, the electron traps begin to fill up, thereby creating the slower complementary grating. Since the field built up by the electron traps is in the direction opposite to that of the hole traps, cancellation of the net

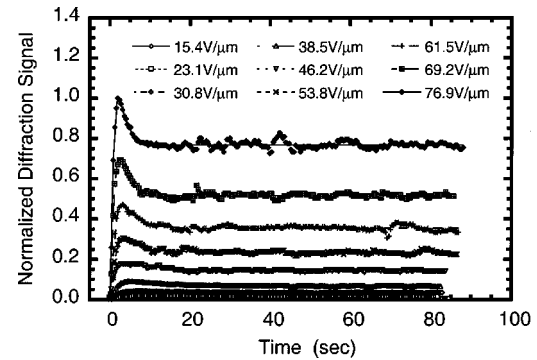


FIG. 9. The temporal evolution of the normalized diffraction efficiency at a different applied field. The writing intensity of each beam was  $760 \text{ mW}/\text{cm}^2$ .

space-charge field and reduction in the diffraction efficiency were observed. When erasing the gratings in the period of stable diffraction, the space-charge field, as formed by the trapped holes, decays faster than that formed by the trapped electrons. Therefore, the net space-charge field changes signs during the erasure process. The diffraction efficiency first decreases to zero and then increases again. A revelation of the diffraction signal was thus observed.

The dynamics of the two sets of gratings were investigated by changing the applied field and irradiation intensity. Figure 9 shows the dynamic behavior of the grating formation in a four-wave mixing experiment. We examined the dynamic behavior at a different applied field with a fixed intensity of  $760 \text{ mW}/\text{cm}^2$ . Obviously, an external field enhanced the formation of both types of grating. This is evidenced by the enhancement of the steady-state diffraction efficiency and the increase in the amount of the cancellation of the diffraction efficiency at a high field. Figure 10 shows the temporal change of the diffraction efficiency at different writing intensities. The experiment was carried out at a fixed applied field of  $77 \text{ V}/\mu\text{m}$ . These data indicate that the diffraction efficiency increases with the writing intensities, yet it tends to be saturated at high intensities.

## IV. HOLE AND ELECTRON TRANSPORT

### A. Time-of-flight experiments

As mentioned above, a crucial condition for the formation of the complementary gratings is the existence of two trans-

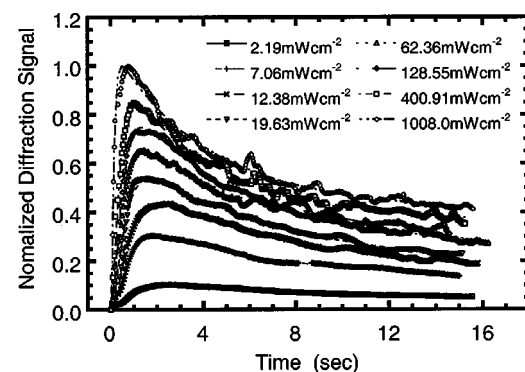


FIG. 10. The temporal evolution of the normalized diffraction efficiency at the different intensity of each writing beam. The applied field was  $77 \text{ V}/\mu\text{m}$ .

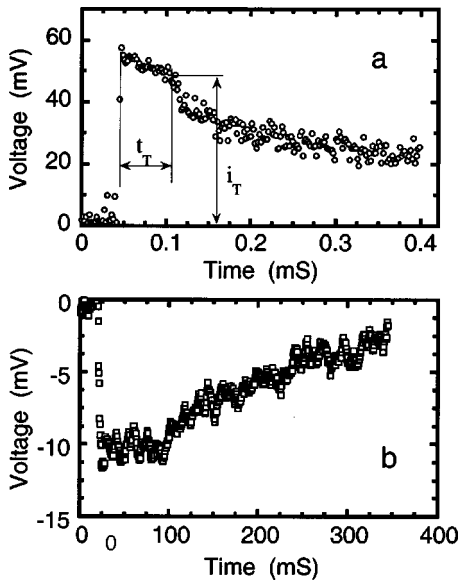


FIG. 11. Two typical time-of-flight signals for hole (a) and electron (b) transport. The  $t_T$  is transit time.

porting channels: one for the migration of electrons and another for the migration of holes. To examine, experimentally, the coexistence of two channels for electron and hole transport, we measured the mobility and the photogeneration efficiency for holes and electrons, respectively, by time-of-flight experiments.<sup>44,46,47</sup>

These measurements were carried out independently as a function of an applied field. For the observation of the time-of-flight signal of holes' transport across a film, a sample of 27  $\mu\text{m}$  thick sandwiched between a piece of ITO glass and an aluminum plate was used. Frequency doubled laser pulses ( $\lambda = 532 \text{ nm}$ ) of about 40 picosec FWHM (full width at half maximum) from a mode-locked Nd:YAG (where YAG denotes yttrium aluminum garnet) laser (Continuum, Model PY61C-10) irradiated the film from the positively charged ITO electrode, while the aluminum electrode was connected to a grounded resistor. Since the absorption coefficient of the material at the working wavelength of 532 nm is about  $7900 \text{ cm}^{-1}$ , a charge carrier sheet approximately  $1.5 \mu\text{m}$  thick was formed beneath the transparent electrode. Under the action of the external field, holes were drifted across the film to the grounded electrode. This resulted in a transient current, which was measured by recording the potential drop across the resistor with a digital oscilloscope (LeCroy, Model 9354A). A typical transient current for the hole transport is shown in Fig. 11(a). The current pulse did not show the rectangular shape, but rather it showed a featureless decay. Since the material is a disordered solid, the generated carriers experienced a distribution of hopping times. Therefore, the carrier packet that was formed as a thin sheet at the front surface of the sample was broadened as it penetrated the bulk. The experimental transit time was determined by  $t_T$  as shown in Fig. 11(a).

According to the photorefractive analyses in the preceding section, electron transport is available in the materials as well. Measurement of the electron mobility confirmed this assumption. The experimental conditions for this measurement were the same as the mobility measurement of holes except that the grounded electrode was another ITO glass

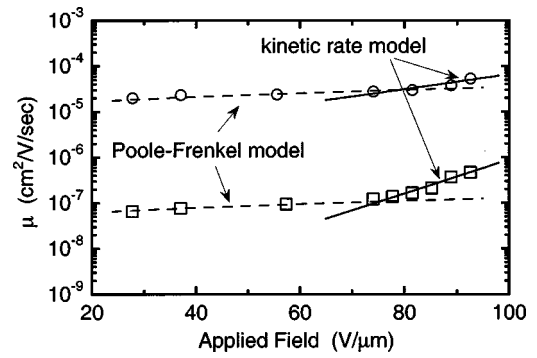


FIG. 12. Hole and electron mobility (circles and squares) as functions of applied field. The dashed and solid lines are best fittings using Eqs. (5) and (6), respectively.

and the front ITO glass electrode was negatively charged. A typical transient current signal for electron transport is shown in Fig. 11(b). The electron transit time is much longer, and the amplitude of the current is also smaller than what was observed in hole transport. This strongly suggests the existence of an electron transport channel in our molecular system.

## B. Mobility of hole and electron

The drift mobilities for hole and electron transport are readily calculated from the transit times  $t_T$  at different external fields using the expression:  $\mu = d^2/Vt_T$ , where  $d$  is the sample thickness and  $V$  is the applied voltage.<sup>44,47,48</sup> The hole and electron drift mobilities as a function of an applied field are depicted in Fig. 12. Both mobilities are strongly enhanced by the applied field. This figure also shows that the enhancement of the electron mobility is more favorable than the enhancement of the hole mobility.

## C. Photogeneration quantum efficiencies

In the external circuit, the drifting charge is manifested as a constant current  $i = Q\mu E/d$ , where  $Q$  is the total charge injected into the sample by the incident light flash  $F$  (absorbed photons per second). Knowing the current  $i_T$  and mobility  $\mu$  [Fig. 10(a)], the quantum efficiency, as defined as the number of carriers generated per absorbed photon, was estimated from the relation of  $\Phi = Q/eF$ , where  $e$  is the electron charge. A strong dependence of the quantum efficiencies for both hole and electron carriers on the applied field was similar to those reported for the disordered materials (Fig. 13). The solid lines are Onsager fittings<sup>49</sup> using the parameters listed within Fig. 13.  $\Phi_0$  is the initial yield of thermalized bound pairs and is independent of field, and  $r_0$  is the thermalization distance.

## V. DISCUSSIONS

### A. Charged-carrier transport channels

Although the competition of complementary gratings explains the experimental data, and the mobility measurements confirm the bipolar transport nature of the material, it was necessary to examine these phenomena at the molecular level. It is also necessary to correlate the photorefractive and charge transport data with a photorefractive model. We used

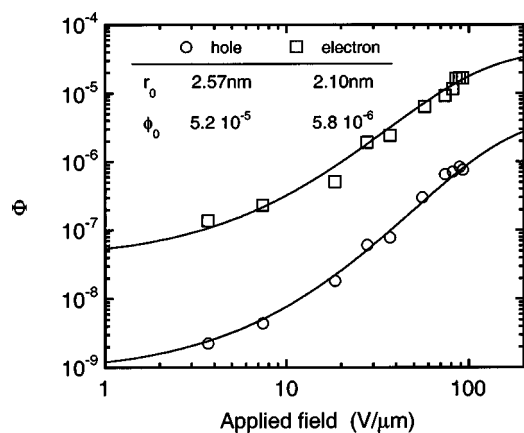


FIG. 13. Photogeneration quantum efficiencies for hole and electron generation. The solid lines are Onsager theory fitting with parameters listed in the figure.

cyclic voltammetry to determine the ionization potential and electron affinity of each component of the molecule in solution.<sup>50</sup> Solution electrochemical measurements can be used to describe electron transfer reactions in the condensed phase if we assume that the differences in ionization potential and electron affinity of the component of the molecule in solution are equal to or smaller than those same energy differences in the condensed phase.<sup>51</sup>

The ionization potentials were deduced from the cyclic voltammetry measurement of the electroactive species at a concentration of  $3 \times 10^{-3}$  mol/dm<sup>3</sup> in dichloromethane solutions containing 0.1 mol/dm<sup>3</sup> tetrabutylammonium tetrafluoroborate as the supporting electrolyte.<sup>41</sup> The ferrocene/ferrocenium-ion couple was used as an internal standard. The HOMO (highest occupied molecular orbital) and LUMO (lowest unoccupied molecular orbital) energy levels were estimated from the equations:  $E_{\text{HOMO}} = E_{\text{ox}}^0 + 4.4$  eV and  $E_{\text{LUMO}} = E_{\text{re}}^0 + 4.4$  eV, where  $E_{\text{ox}}^0$  and  $E_{\text{re}}^0$  are oxidation and reduction potentials with respect to the standard hydrogen electrode, and the value of 4.4 is the ionization potential for hydrogen in eV.<sup>52,53</sup> We characterized the band gaps of the three compounds spectroscopically by finding their band edges, which are also listed in Table I.

The HOMO and LUMO energy levels of the methine dye (Compound 3 in Table I) were calculated to be  $-5.82$  and  $-3.48$  eV, respectively, with respect to the vacuum level, from its lowest oxidation and reduction potentials. The band gap  $\Delta E_{\text{electrochemical}}$  was estimated to be 2.34 eV. This value is in good agreement with the spectroscopic estimate of the band gap  $\Delta E_{\text{optical}}$ , 2.30 eV. The HOMO energy of a sexithiophene molecule alone (Compound 2) was estimated to be  $-5.48$  eV. Since the reduction potential of sexithiophene is out of the solvent window, the LUMO energy level ( $-3.00$  eV) was deduced from the band gap of the sexithiophene backbone, which was estimated from the photoabsorption edge (2.48 eV). If we assume that there is no ground-state intramolecular interaction between the sexithiophene backbone and the methine dye, the energy levels in our photorefractive molecule should remain identical to their individual components. Indeed, the HOMO and LUMO energy levels for the photorefractive molecules (Compound 1) were electrochemically determined to be  $-5.42$  and  $-3.48$  eV, respectively (Table 1). These are close

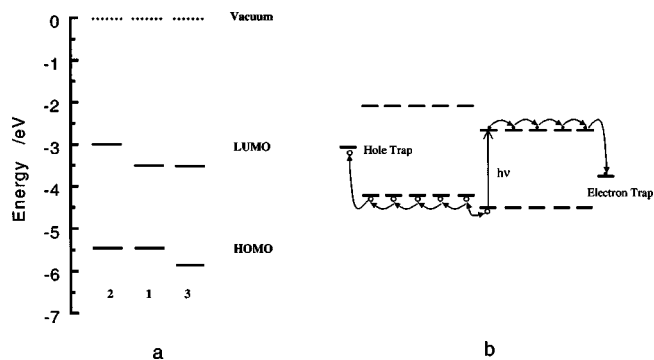


FIG. 14. (a) Estimated energy levels of HOMO and LUMO for a fully functionalized photorefractive molecule (Compound 1), a sexithiophene derivative (Compound 2), and methine dye (Compound 3) with respect to the vacuum level. (b) Proposed charge-carrier transport channels. See text for details.

to those of the individual compounds. A potential energy diagram can be constructed, as shown in Fig. 14(a). A photogeneration of charge carriers occurs upon absorption of a photon by the dye. An electron can be transported away along the LUMO of the methine dye, and the hole tends to transfer to sexithiophene HOMO under the action of an external field. The holes and electrons are further drifted away by sequential hopping to neighboring sexithiophene backbones and methine dyes and can be fixed by individual trapping centers, respectively [Fig. 14(b)].

## B. Bipolar two-trap models

There are several photorefractive models that account for the bipolar transport. A recent review of these models is provided in Ref. 2. The model most consistent with our experimental results is the bipolar two-trap model, which is based on the assumption that two types of active centers are involved in simultaneous electron-hole transport.<sup>34,37,38</sup> This model has been used for the interpretation of the behaviors of complementary gratings in inorganic photorefractive crystals. According to this model, there are two independent systems of photoactive centers in which the prevailing carriers are electrons and holes, respectively. One of the gratings is set up by the redistribution of electrons, and another is set up by the redistribution of holes. The two gratings are  $180^\circ$  out of phase with each other and are known as complementary gratings. Since the total space-charge field is the sum of the fields created by each type of carrier caught by different traps, the net amplitude of the space-charge field is smaller than that of the contribution from the principal set of space charges. If their characteristic time constants are different, then the individual gratings can be revealed during writing and erasure.

The model predicts an expression for the steady-state space-charge field as<sup>34</sup>

$$E_{SC} = j \frac{E_{qD} - E_{qA}}{1 + j \frac{E_{qD}}{E_0 + jE_D} - j \frac{E_{qA}}{E_0 - jE_D}}, \quad (2)$$

where

$$E_D = \frac{k_B T}{e} K,$$

$$E_{qD} = \frac{e}{\epsilon_s K} \frac{(N_D - N_{D0}^+) N_{D0}^+}{N_D},$$

and

$$E_{qA} = \frac{e}{\epsilon_s K} \frac{(N_A - N_{A0}^-) N_{A0}^-}{N_A},$$

are the diffusion field, the trap-limited space-charge fields of  $N$ -type, and the  $P$ -type species, respectively.  $N_{A0}^- = N_{D0}^+$ ,  $k_B$  is the Boltzmann's constant,  $T$  is the absolute temperature,  $K$  is the spatial frequency of grating,  $e$  is the charge of the electron,  $\epsilon_s$  is the static dielectric permittivity, and  $N_D$ ,  $N_A$ ,  $N_{D0}^+$ ,  $N_{A0}^-$  are the total concentration of donors and acceptors and the concentration of ionized donors and acceptors, respectively. The  $E_D$  value is 0.16 V/ $\mu\text{m}$  at a 1  $\mu\text{m}$  grating spacing and room temperature and is much smaller than the applied field in our experiments (which is the case for the most organic photorefractive films). Under the condition of  $E_0 \gg E_D$ , Eq. (2) can be expressed as

$$E_{SC} = \frac{E_{q\text{eff}}(E_0 - jE_D)}{E_D + E_{q\text{eff}} + jE_0}, \quad (3)$$

where  $E_{q\text{eff}} = E_{qA} - E_{qD}$ . Equation (3) is the same formula as the "standard model of photorefraction",<sup>22</sup> when the one species trap-limited field  $E_q$  is replaced with an effective trap-limited field  $E_{q\text{eff}}$ . Therefore, the bipolar two-trap model predicts the same steady-state photorefractive behaviors as the standard model. Equation (3) explains the reason why the field and grating spacing dependences of the gain coefficient and the diffraction efficiency (Figs. 2–5) are similar to those reported in the monopolar polymeric and molecular photorefractive materials. Fitting Equation (3) into the gain coefficient and the diffraction efficiency data (solid lines in Figs. 2–5) results in the effective trap-limited field  $E_{q\text{eff}} = 94.5 - 103.0$  V/ $\mu\text{m}$ . The sign of the space-charge field and, therefore, the direction of the energy transfer, depends merely on the sign of field  $E_{q\text{eff}}$ , which is determined by the relative density of the donor and acceptor traps. Varying the grating spatial frequency cannot change the sign of the steady-state space-charge fields. On the contrary, in the bipolar single-trap model, the steady-state gain coefficient can change signs with the grating period. This is because the phase of the space-charge field depends on the uncoupled response time of the electron- and the hole-transport processes.<sup>54,55</sup> Therefore, the space-charge fields formed by trapped electrons and holes cannot be determined individually from measuring the steady-state properties; however, the time-dependent measurements can accomplish this function.

The sign of the space-charge field, and hence the direction of energy transfer in the bipolar two-trap model, can change with time during the writing and erasure of complementary gratings. The condition is that their characteristic time constants must be different. The sign of the space-charge field in the erasing process depicted in Fig. 8 must change after the dip, since the diffraction efficiency is proportional to the square of the space-charge field. The time for the dip was

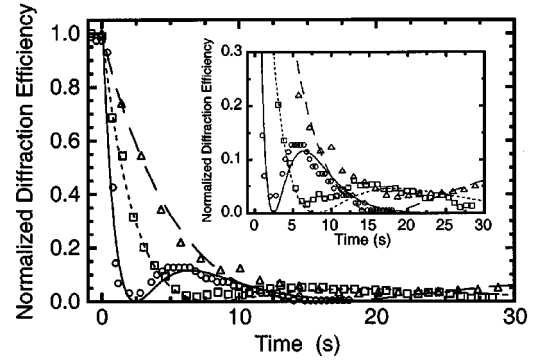


FIG. 15. Normalized diffraction efficiency as a function of time during the grating erasure. The circles, squares, and triangles are experimental measurements with the grating spacing of 1.1, 1.9, and 4.4  $\mu\text{m}$ , respectively, at an applied field of 77 V/ $\mu\text{m}$ . The lines are theoretical fits using a biexponential function [Eq. (4)]. The inset is its enlarged plot.

delayed when the grating spacing increased as shown in Fig. 15, where dips appeared at about 2.5, 7.3, and 20.0 sec of erasure time for the gratings with spacing of 1.1, 1.9, and 4.4  $\mu\text{m}$ , respectively. The sign of the space-charge field did not change in the writing process in Fig. 8 for two reasons: firstly, because the space-charge field contributed from the hole was dominated, and secondly, because the buildup time constant for the hole grating was faster than that for the electron grating. We also did not observe a diffraction efficiency dip during the grating writing process in the spacing range from 0.4 to 4.5  $\mu\text{m}$ . This would be possible under certain conditions, according to the bipolar two-species models, for example, if the response rate for electrons becomes smaller than the rate for holes during the variation of the grating spacing.<sup>34,54</sup> In contrast to the case in the bipolar two-trap model, the grating formation and erasure in the one-species electron-hole competition model follow single exponential functions.<sup>54–56</sup>

The expression for the writing and erasing diffraction efficiency is<sup>34,37</sup>

$$\eta(t) \propto \left| E_e \left[ 1 - \exp\left(-\frac{t}{\tau_e}\right) \right] - E_h \left( 1 - \exp\left(-\frac{t}{\tau_h}\right) \right) \right|^2,$$

and

$$\eta(t) \propto \left| E_e \exp\left(-\frac{t}{\tau_e}\right) - E_h \exp\left(-\frac{t}{\tau_h}\right) \right|^2, \quad (4)$$

where  $E_e$  and  $E_h$  are the steady-state space-charge fields built up by the trapped electrons and holes, and  $\tau_e$  and  $\tau_h$  are the time constants for the electron- and hole-transport systems. Fitting the data according to the writing and erasure processes into Eq. (4) yielded the lines in Figs. 8 and 15.

This model requires a zero diffraction efficiency dip during erasure due to the 180° phase difference of the complementary gratings. Since the space-charge field is completely canceled at the dip, a nonzero dip can be observed only when there is a slight phase shift in the complementary gratings. This phase shift can be due to either the vibration during hologram recording<sup>37</sup> or to the simultaneous appearance of photochromic or absorption grating.<sup>57</sup> In our experiments, a



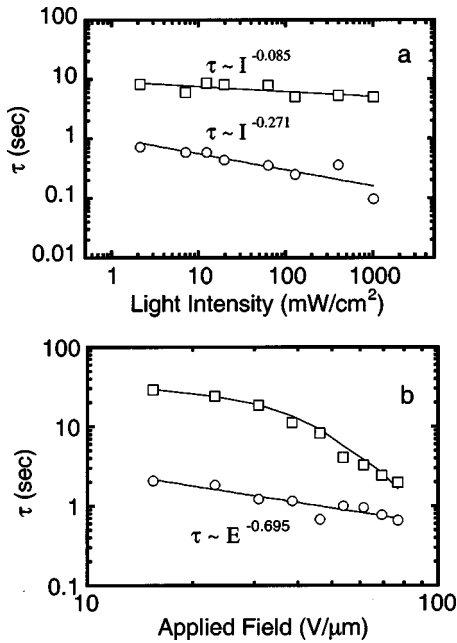


FIG. 16. Time constants for buildup of a fast grating (circles) and a slow complementary grating (squares) as functions of illumination light intensity (a) and applied field (b).

nonzero dip was observed only when the measurements were performed under noisier conditions.

Although similar grating cancellation and revelation behavior has been observed in other photorefractive polymeric composites, it was attributed either to the trap's intercommunication or to residual ionic motion.<sup>28-30</sup> However, the complementary gratings that are reported in this paper are formed by the space-charge field of two types of photogenerated charge carriers.

### C. Grating dynamics

Figure 16 shows the influence of the writing beam intensity and applied field on the buildup dynamics of the primary grating and its complementary grating ( $\tau_e$ , and  $\tau_h$ ). Figure 14(a) shows time constants ( $\tau_e$  and  $\tau_h$ ) as a function of the writing beam intensity and indicates that both time constants decrease with increased intensity. Figure 17 shows the relationships of the magnitude fraction of the slow component of a space-charge field, defined as  $r_{\text{slow}} = E_e / (E_e + E_h)$  with the writing beam intensity and the applied field. The  $\tau_e$ ,  $\tau_h$ ,  $E_e$ , and  $E_h$  values were obtained by fitting Eq. (4) into the dynamic data in Figs. 9 and 10. The standard photorefractive theory predicts that the time constant is inversely proportional to the carrier mobility and the intensity of the writing beams (time constant  $\propto 1/\text{mobility} \times \text{intensity}$ ) (Refs 11 and 58). However, the dependence of time constants on the light intensity of both holes and electrons is much weaker than the above relationship and those reported in other organic and inorganic monopolar transport materials.<sup>3,4,14,29,59</sup> In this low- $T_g$  photorefractive material, the fast component of response times can be hindered by the NLO reorientation besides the space-charge field formation. This is because the NLO reorientation speed in the rubbery state of amorphous matrix is independent of the light intensity<sup>60</sup> yet controlled by the diffusion constant.<sup>61</sup> Therefore, fast grating formation

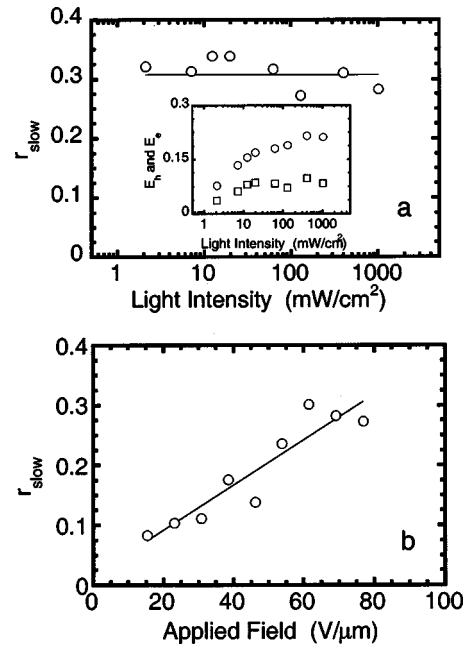


FIG. 17. Magnitude fraction of slow grating  $r_{\text{slow}} = E_e / (E_e + E_h)$  as functions of illumination light intensity (a) and applied field (b). The inset in (a) is the  $E_e$  and  $E_h$  as a function of light intensity.

can be subjected to the hindrance from the reorientation motion of NLO chromophores. The field-induced birefringence measurement shows that the time constants for the buildup of the index birefringence under the action of external fields are in the same order as the fast component of the response time of the grating formation.<sup>41</sup> Though the slow electron grating is not hindered by the NLO reorientation, it has an even weaker dependence on the light intensity than the fast grating. This slowing down could come from the interaction between the complementary gratings. The principal space-charge field buildup by holes accelerates the migration of the slow complementary grating. As a result, the interaction force weakens the effect of the light intensity on the time constant of the slow grating.

In order to understand the applied field dependence behaviors of time constants more deeply, let us consider further the field dependence of carrier mobility shown in Fig. 12. The field dependence of the mobility in disordered organic films has been described by the Poole-Frenkel effect, kinetic rate models, the Marcus theory, the dipole trap argument, and by disordered formalism.<sup>44</sup> It was found that none of the above theories covers the whole range of the field measured. It was further noticed that in the low-field range of  $E < 70$  V/ $\mu$ m, the mobilities show much weaker dependence on the field and follow the relationship predicted by the Poole-Frenkel effect. At a high field range ( $70 < E < 100$  V/ $\mu$ m), the data can be well fitted into the kinetic rate theory. This inconsistency in the mechanisms throughout the measurement range can be attributed to a quasimorphology difference at different applied fields as a result of the low- $T_g$  nature of the material. The chromophores are more randomized at a low field than at a high field. The Poole-Frenkel effect describes the reduction in the ionization energy of a carrier in a Coulomb potential by an applied field. The dependence of the mobility on a field can be expressed as<sup>44</sup>

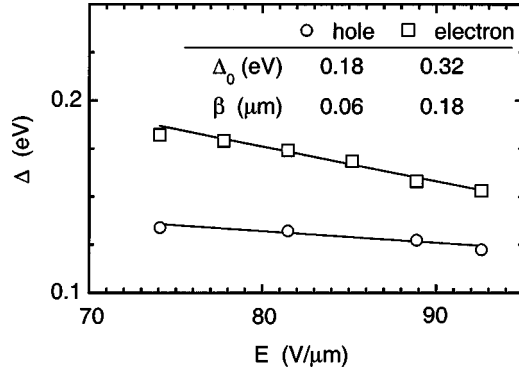


FIG. 18. The activation energy for hole (squares) and electron (circles) hopping.

$$\mu = \mu_0 \exp(\beta_{PF} E^{1/2} / kT), \quad (5)$$

where  $\beta_{PF} = (e^3 / \pi \epsilon \epsilon_0)^{1/2}$ ,  $\epsilon$  is the dielectric constant at high frequency, and  $\epsilon_0$  is the permittivity of free space. The kinetic rate theory assumes that the electron and hole transports occur by hopping among the localized states, and the mobility can be adopted as<sup>44,47</sup>

$$\mu = 2 \frac{\rho}{E} \nu \exp\left(-\frac{\Delta(E)}{kT}\right) \sinh\left(\frac{\rho e E}{2kT}\right), \quad (6)$$

where  $\rho$  is the average separation of the transporting agents,  $\nu$  is the attempt frequency of electron-exchange between charged and uncharged localized discrete chemical species,  $\Delta(E) = \Delta_0 - \beta E$  is the activation energy for the hopping process, and  $\Delta_0$  is the zero field intercept.<sup>62</sup> The dashed and solid lines of Fig. 12 are the best fitting results, using Eqs. (5) and (6), respectively. In the fitting, the dielectric constant  $\epsilon$  is assumed to be 3.0, and the average distance value  $\rho$  for both hole and electron transport species is 13.9 Å. It is calculated from the formula  $\rho = [M / (Ad)]^{1/3}$ , where  $M$  is the molecular weight of photorefractive sexithiophene (1946.16),  $d$  is the density (1.2) and  $A$  is Avogadro's number ( $6.02 \times 10^{23}$ ). The resultant zero field intercept  $\Delta_0$  and  $\beta$  values are listed as an inset in Fig. 18. The activation energies for both holes and electrons are slightly dependent on the external field, but the electron has a larger  $\Delta$  value than the hole and is more strongly influenced by the external field (Fig. 18). While the  $\beta$  value for electron hopping is larger than for hole hopping, the activation energy for electron hopping decreases faster with the applied field than for the hole hopping. As a result, the time constant of slow grating at a high-applied field is more sensitive to the changes in the applied field than that of the fast grating (Fig. 16). This is because the mobility follows the kinetic rate theory at a high-applied field (Figure 12). The  $r_{\text{slow}}$  value reflects the relation of the two gratings at steady-state conditions.

Figure 17(a) shows the  $r_{\text{slow}}$  value as a function of the intensity of the writing beam at a constant applied field ( $E_{\text{applied}} = 77 \text{ V}/\mu\text{m}$ ). It can be seen that the  $r_{\text{slow}}$  values remain almost unchanged over a variation in the intensity span almost three orders of magnitude. Meanwhile, the absolute space-charge field magnitude of the fast component,  $E_h$ , triples in value, and a saturation of the space-charge fields,  $E_e$  and  $E_h$ , appears at a writing intensity of about  $I_w = 50 \text{ mW}/\text{cm}^2$  [see the inset of Fig. 17(a)]. It can be readily

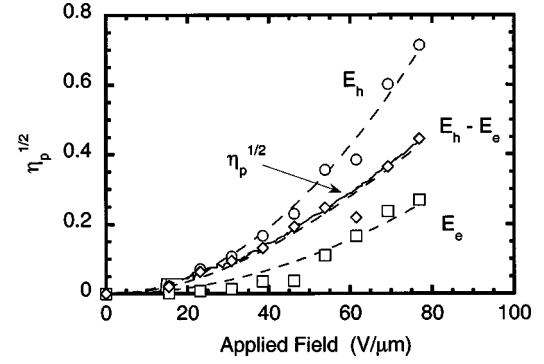


FIG. 19. The  $E_e$  and  $E_h$  (squares and circles), as well as the  $E_h - E_e$  value and square root of diffraction efficient (diamonds and solid line) as a function of light intensity.

understood that  $r_{\text{slow}}$  is invariable when  $I_w > 50 \text{ mW}/\text{cm}^2$  because both space-charge field components from trapped electrons and holes reach their individual trap limitation conditions as indicated by Eq. (2). For the case of  $I_w < 50 \text{ mW}/\text{cm}^2$ , the  $r_{\text{slow}}$  remains constant because the relation of the photoexcited electron and hole densities remains constant, and because the space-charge field built up by each carrier still depends on the density of two types of traps. On the other hand, the  $r_{\text{slow}}$  value increases when the applied field increases at a constant light intensity ( $I_w = 760 \text{ mW}/\text{cm}^2$ ) as shown in Fig. 17(b). This trend is consistent with Eq. (2) because under the condition of  $E_{qD} > E_{qA}$ , the trap-density-limited space-charge field due to trapped electrons depends more strongly on the applied field than the trapped holes.

Equation (2) reveals that the overall space charge field is, in fact, a superposition of two space-charge fields from two types of trapped charges. Our results indeed confirm this prediction (Fig. 19). Agreement is observed between  $\sqrt{\eta}$  and  $E_h - E_e$ . The dashed lines are the fitting by Eq. (3).

It is important to point out that the complementary grating observed in our sexithiophene photorefractive materials is not due to a passive motion of residual ions as described in Ref. 30. If the complementary grating originated from this reason, the  $r_{\text{slow}}$  value in Fig. 17(a) could not have remained constant. The space-charge field from ions should always satisfy the trap density limitation condition, since the number density of ions is independent of light intensity.

This assertion is supported by photocurrent measurement results, as shown in Fig. 20. It is indicated that the photocur-

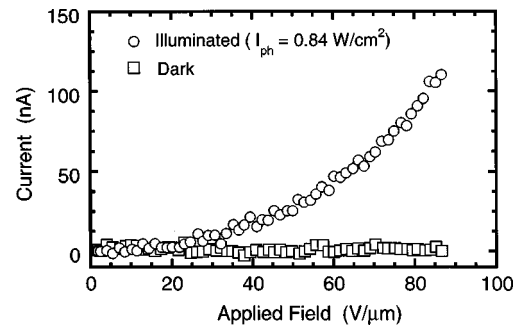


FIG. 20. Photo- and dark current measured from a 27- $\mu\text{m}$ -thick sample.

rent increases superlinearly with the applied field, while the dark current remains zero as the external field is increased up to  $90 \text{ V}/\mu\text{m}$ . The revelation effect that we observed should not be attributed to the appearance of a monopolar shallow trap<sup>63</sup> because the diffraction efficiency dipped to zero under uniform illumination. This is not the case for the shallow trap model.<sup>64</sup> An oscillation on the space-charge field in monopolar photorefractive materials can happen at the initial stages of grating formation and erasure.<sup>65,66</sup> The “density” gratings of the photoexcited carriers drift along the grating vector direction under the action of a high external field. If the drift length is longer than the grating space, then the rise and fall of the amplitude of the Coulomb electric field grating can be observed before significant diffusion takes place. This is caused by the movement of the carrier grating from  $0^\circ$  to  $180^\circ$  and back to the in phase with the stationary grating of ionized traps.<sup>65</sup> This kind of oscillation is not complete and will be dampened due to carrier recombination. A zero dip similar to the complementary grating competition cannot be observed.

## VI. CONCLUSIONS

The sexithiophene derivative with an NLO chromophore as described has shown high photorefractive sensitivity with a sizable photorefractive gain and diffraction efficiency. The special properties of competition between two complementary charge gratings were observed. Although the phenomena have been extensively studied experimentally and theo-

retically in inorganic materials, this is the first detailed study, to the best of our knowledge, in organic material. Our study justified the bipolar charge carrier transport model and illustrated its effect on photorefractive properties.

The bipolar transport model is supported by time-of-flight experiments. The energy levels of HOMO and LUMO of hole and electron transport components, which correspond to the sexithiophene backbone and the NLO chromophore, were evaluated from cyclic voltammetry and photoabsorption spectroscopic measurements. The intrinsic *p-n* junction-like energy levels within a single molecule were shown to support the mechanisms of the simultaneous hole and electron transport. The differences in mobility and trap depth cause the buildup and erasing processes to have different time constants for electron and hole systems. Therefore, the cancellation, revelation, and oscillationlike behaviors of the gratings were observed. The dynamic parameters of the grating-writing process and the steady-state properties were consistently explained.

## ACKNOWLEDGMENTS

This work was supported by the National Science Foundation and the Air Force Office of Scientific Research. This work also benefited from NSF support through the MRSEC program at the University of Chicago. The authors thank Mr. B. Houseman for proofreading the manuscript and giving his suggestions.

Email address: luping@midway.uchicago.edu

<sup>1</sup>*Photorefractive Materials and Their Applications*, edited by P. Günter and J. P. Huignard (Springer, New York, 1988), Vols. 1 and 2.

<sup>2</sup>L. Solymar, D. J. Webb, and A. Grunnet-Jepsen in *The Physics and Application of Photorefractive Materials*, edited by A. Hasegawa, M. Lapp, B. B. Snively, H. Stark, A. C. Tam, and T. Wilson (Clarendon Press, Oxford, 1996).

<sup>3</sup>P. Günter, *Phys. Rep.* **93**, 199 (1982).

<sup>4</sup>W. E. Moerner and S. M. Silence, *Chem. Rev.* **94**, 127 (1994); W. E. Moerner, A. Grunnet-Jepsen, and C. L. Thompson, *Annu. Rev. Mater. Sci.* **27**, 585 (1997).

<sup>5</sup>L. P. Yu, W. K. Chen, Z. H. Peng, and A. R. Gharavi, *Acc. Chem. Res.* **29**, 13 (1996).

<sup>6</sup>S. Ducharme, J. C. Scott, R. J. Twieg, and W. E. Moerner, *Phys. Rev. Lett.* **66**, 1846 (1991).

<sup>7</sup>K. Meerholz, B. L. Volodin, Sanalphon, B. Kippelen, and N. Peyghambarian, *Nature (London)* **371**, 497 (1994).

<sup>8</sup>B. Kippelen, S. R. Marder, E. Hendrichy, J. L. Maldonado, G. Guillemet, B. L. Volodin, D. D. Steele, Y. Edami, Sanalphon, Y. J. Yao, J. F. Wang, H. Röchel, L. Erskine, and N. Peyghambarian, *Science* **279**, 54 (1998).

<sup>9</sup>A. M. Cox, R. D. Blackburn, D. P. West, T. A. King, F. A. Wade, and D. A. Leigh, *Appl. Phys. Lett.* **68**, 2801 (1996).

<sup>10</sup>E. Hendrickx, J. Herlocker, J. L. Maldonado, S. R. Marder, B. Kippelen, A. Persoons, and N. Peyghambarian, *Appl. Phys. Lett.* **72**, 1679 (1998).

<sup>11</sup>A. Grunnet-Jepsen, C. L. Thompson, R. J. Twieg, and W. E. Moerner, *Appl. Phys. Lett.* **70**, 1515 (1997).

<sup>12</sup>P. M. Lundquist, R. Wortmann, C. Geletneky, R. J. Twieg, M.

Jurich, V. Y. Lee, C. R. Moylan, and D. M. Burland, *Science* **274**, 1182 (1996).

<sup>13</sup>Z. Peng, A. R. Gharavi, and L. Yu, *Appl. Phys. Lett.* **69**, 4002 (1996).

<sup>14</sup>Qing Wang, Liming Wang, Haythem Saadeh, and Luping Yu, *Chem. Commun. (Cambridge)* **17**, 1689 (1999).

<sup>15</sup>W. J. Li, A. Gharavi, Q. Wang, and P. L. Yu, *Adv. Mater.* **10**, 927 (1998).

<sup>16</sup>K. Ogino, S. H. Park, and H. Sato, *Appl. Phys. Lett.* **74**, 3936 (1999).

<sup>17</sup>L. Wang, Y. Zhang, T. Wada, and H. Sasabe, *Appl. Phys. Lett.* **69**, 728 (1996).

<sup>18</sup>S. Schloter, A. Schreiber, M. Grasruck, A. Leopold, M. Kol'chenko, J. Pan, C. Hohl, P. Strohsriegl, S. J. Zilker, and D. Haarer, *Appl. Phys. B: Photophys. Laser Chem.* **68**, 899 (1999).

<sup>19</sup>A. Grunnet-Jepsen, C. L. Thompson, R. J. Twieg, and W. E. Moerner, *J. Opt. Soc. Am. B* **15**, 901 (1998).

<sup>20</sup>P. M. Lundquist, C. Popa, R. G. DeVoe, Y. Jia, and W. E. Moerner, *Opt. Lett.* **21**, 890 (1996).

<sup>21</sup>B. L. Volodin, B. Kippelen, K. Meerholz, B. Javidi, and N. Peyghambarian, *Nature (London)* **383**, 58 (1996).

<sup>22</sup>By “standard model of photorefraction,” we refer to the model that initially was developed by Kukhtarev and coworkers [N. V. Kukhtarev, V. B. Markov, and S. G. Odulov, *Opt. Commun.* **23**, 338 (1977); N. V. Kukhtarev, V. B. Markov, S. G. Odulov, M. S. Soskin, and V. L. Vinetskii, *Ferroelectrics* **22**, 949 (1979); **22**, 961 (1979); N. V. Kukhtarev, *Sov. Tech. Phys. Lett.* **2**, 438 (1976)] and later modifications. The model considered the monopolar band transport and one-trap level. The expansions of the model that consider such effects as multiple trap levels and si-

- multaneous electron and hole transporting are not included. A good summary of these models has been given in Ref. 2.
- <sup>23</sup>K. Okamoto, T. Nomura, S. H. Park, K. Ogino, and H. Sata, *Chem. Mater.* **11**, 3279 (1999).
- <sup>24</sup>C. Hohle, U. Hofmann, S. Schloter, M. Thelakkat, P. Stroehriegl, D. Haarer, and S. J. Zilker, *J. Mater. Chem.* **9**, 2205 (1999); S. Schloter, A. Schreiber, M. Gräsrunk, A. Leopold, M. Kol'chenko, J. Pan, C. Hohle, P. Stroehriegl, S. J. Zilker, and D. Haarer, *Appl. Phys. B: Lasers Opt.* **68**, 899 (1999).
- <sup>25</sup>R. Bitter, C. Bräuchle, and K. Meerholz, *Appl. Opt.* **37**, 2843 (1998); F. Wüthner, R. Wortmann, R. Matschiner, K. Lukaszuk, K. Meerholz, Y. DeNardin, R. Bittner, C. Bräuchle, and R. Sens, *Angew. Chem. Int. Ed. Engl.* **36**, 2765 (1997).
- <sup>26</sup>F. Nishida and Y. Tomita, *J. Appl. Phys.* **7**, 55 (1997).
- <sup>27</sup>Q. Wang, L. Wang, and L. P. Yu, *J. Am. Chem. Soc.* **120**, 12 860 (1998).
- <sup>28</sup>S. Ducharme, B. Jones, J. M. Takacs, and L. Zhang, *Opt. Lett.* **18**, 152 (1993).
- <sup>29</sup>S. M. Silence, R. J. Twieg, G. C. Bjorklund, and W. E. Moerner, *Phys. Rev. Lett.* **73**, 2047 (1994).
- <sup>30</sup>S. M. Silence, C. A. Walsh, J. C. Scott, T. J. Matray, R. J. Twieg, F. Hache, G. C. Bjorklund, and W. E. Moerner, *Opt. Lett.* **17**, 1107 (1992).
- <sup>31</sup>E. Krätzig, *Ferroelectrics* **21**, 635 (1978); R. Orlowski and E. Krätzig, *Solid State Commun.* **27**, 1351 (1978); X. Xue, E. Krätzig, and R. Rupp, *J. Opt. Soc. Am. B* **15**, 2383 (1998).
- <sup>32</sup>N. Barry, L. Duffault, R. Troth, R. Ramos-Garcia, and M. Damzen, *J. Opt. Soc. Am. B* **11**, 1758 (1994).
- <sup>33</sup>M. Miteva and L. Nikolova, *Opt. Commun.* **67**, 192 (1988).
- <sup>34</sup>S. Zhivkova and M. Miteva, *J. Appl. Phys.* **68**, 3099 (1990).
- <sup>35</sup>E. Rickerman, S. Riehemann, K. Buse, D. Dirksen, and G. von Bally, *J. Opt. Soc. Am. B* **13**, 2299 (1996).
- <sup>36</sup>S. G. Odoulov, A. N. Shumelyuk, U. Hellwig, R. A. Rupp, A. A. Grabar, and I. M. Stoyka, *J. Opt. Soc. Am. B* **13**, 2352 (1996).
- <sup>37</sup>M. C. Bashaw, T.-P. Ma, R. C. Baker, S. Mroczkowski, and R. R. Dube, *J. Opt. Soc. Am. B* **7**, 2329 (1990); M. C. Bashaw, T.-P. Ma, R. C. Baker, S. Mroczkowski, and R. R. Dube, *Phys. Rev. B* **42**, 5641 (1990).
- <sup>38</sup>G. C. Valley, *J. Appl. Phys.* **59**, 3363 (1986).
- <sup>39</sup>E. Strohkendl, J. Jonathan, and R. W. Hellwarth, *Opt. Lett.* **11**, 312 (1986).
- <sup>40</sup>M. C. Bashaw, M. Jeganathan, and L. Hesselink, *J. Opt. Soc. Am. B* **11**, 1743 (1994).
- <sup>41</sup>Man-Kit Ng, Liming Wang, and Luping Yu, *Chem. Mater.* (to be published).
- <sup>42</sup>W. E. Moerner, S. M. Silence, F. Hache, and G. C. Bjorklund, *J. Opt. Soc. Am. B* **11**, 320 (1994).
- <sup>43</sup>K. Sutter and P. Günter, *J. Opt. Soc. Am. B* **7**, 2274 (1990).
- <sup>44</sup>For a recent review, see P. M. Borsenberger and D. S. Weiss, in *Organic Photoreceptors for Xerography*, edited by B. J. Thompson (Marcel Dekker, New York, 1998).
- <sup>45</sup>X. Yue, J. Xu, F. Mersch, R. Rupp, and E. Krätzig, *Phys. Rev. B* **55**, 192 (1988).
- <sup>46</sup>W. D. Gill, *J. Appl. Phys.* **43**, 5033 (1972).
- <sup>47</sup>M. Stoka, J. F. Yanus, and D. M. Pai, *J. Phys. Chem.* **88**, 4707 (1984).
- <sup>48</sup>J. Mort, G. Pfister, and S. Grammatica, *Solid State Commun.* **18**, 693 (1976).
- <sup>49</sup>L. Onsager, *Phys. Rev.* **54**, 554 (1938).
- <sup>50</sup>H. Meng, W. L. Yu, and W. Huang, *Macromolecules* **32**, 8841 (1999).
- <sup>51</sup>J. D. Anderson, E. M. Mconald, P. A. Lee, M. L. Anderson *et al.*, *J. Am. Chem. Soc.* **120**, 9646 (1998).
- <sup>52</sup>W. C. Barrette, Jr., H. W. Johnson, and D. T. Sawyer, *Anal. Chem.* **56**, 1890 (1984).
- <sup>53</sup>H. Reiss and A. Heller, *J. Phys. Chem.* **89**, 4207 (1985).
- <sup>54</sup>M. C. Bashaw, T.-P. Ma, and R. C. Baker, *J. Opt. Soc. Am. B* **9**, 1666 (1992), and references cited therein.
- <sup>55</sup>M. B. Klein and G. C. Valley, *J. Appl. Phys.* **57**, 4901 (1985).
- <sup>56</sup>D. Rytz, B. A. Wechsler, M. H. Garrett, C. C. Nelson, and R. N. Schwartz, *J. Opt. Soc. Am. B* **7**, 2245 (1990).
- <sup>57</sup>L. M. Bernardo, J. C. Lopez, and O. C. Soares, *Appl. Opt.* **29**, 12 (1990).
- <sup>58</sup>G. C. Valley and M. B. Klein, *Opt. Eng. (Bellingham)* **22**, 704 (1983).
- <sup>59</sup>Y. Zhang, C. A. Spencer, S. Ghosal, M. K. Casstevens, and R. Burzynski, *J. Appl. Phys.* **76**, 671 (1994).
- <sup>60</sup>D. Wright, M. A. Díaz-García, J. D. Caspersen, M. DeClue, W. E. Moerner, and R. J. Twieg, *Appl. Phys. Lett.* **73**, 1490 (1998).
- <sup>61</sup>J. W. Wu, *J. Opt. Soc. Am. B* **8**, 142 (1991).
- <sup>62</sup>G. Pfister, *Phys. Rev. B* **16**, 3676 (1977).
- <sup>63</sup>“Shallow” traps are traps from which electrons or holes may be excited thermally.
- <sup>64</sup>P. Tayebati, *J. Appl. Phys.* **70**, 4082 (1991).
- <sup>65</sup>J. P. Partanen, J. M. Jonathan, and R. W. Hellwarth, *Appl. Phys. Lett.* **57**, 2404 (1990); J. P. Partanen, P. Nouchi, J. M. Jonathan, and R. W. Hellwarth, *Phys. Rev. B* **44**, 1487 (1991).
- <sup>66</sup>G. G. Mailliaras, V. V. Krasnikov, H. J. Bolink, and G. Hadziioannou, *Appl. Phys. Lett.* **67**, 455 (1995).